Effects of molecular shape and flexibility on fast sound of organic liquids

Tsuyoshi Yamaguchi, Koji Yoshida, Shinya Hosokawa, et al.

View Online **Export Citation** **CrossMark**

ARTICLES YOU MAY BE INTERESTED IN

Charge transfer at finite temperature: The "$|\Delta\mu|$ big is good" principle
The Journal of Chemical Physics **157**, 156101 (2022); https://doi.org/10.1063/5.0107355

Conductance of concentrated electrolytes: Multivalency and the Wien effect
The Journal of Chemical Physics **157**, 154502 (2022); https://doi.org/10.1063/5.0111645

Guiding the self-assembly of colloidal diamond
The Journal of Chemical Physics **157**, 154503 (2022); https://doi.org/10.1063/5.0109377

Effects of molecular shape and flexibility on fast sound of organic liquids

View Online   Export Citation   CrossMark

Tsuyoshi Yamaguchi,[1,a] (iD)   Koji Yoshida,[2] (iD)   Shinya Hosokawa,[3] (iD)   Daisuke Ishikawa,[4,5] (iD)
and Alfred Q. R. Baron[4,5] (iD)

AFFILIATIONS

[1] Graduate School of Engineering, Nagoya University, Chikusa, Nagoya 464–8603, Japan
[2] Department of Chemistry, Fukuoka University, 8-19-1 Nanakuma, Jonan-ku, Fukuoka 814-0180, Japan
[3] Institute of Industrial Nanomaterials, Kumamoto University, 2-39-1 Kurokami, Chuo-ku, Kumamoto 860-8555, Japan
[4] Materials Dynamics Laboratory, RIKEN SPring-8 Center, RIKEN, Sayo, Hyogo 679-5148, Japan
[5] Precision Spectroscopy Division, CSRR, SPring-8/JASRI, Sayo, Hyogo 679-5198, Japan

[a] Author to whom correspondence should be addressed: yamaguchi.tsuyoshi@material.nagoya-u.ac.jp

ABSTRACT

Inelastic x-ray scattering spectra of four organic liquids, n-hexane, cyclohexane, ethylene glycol dimethyl ether, and 1,4-dioxane, were measured, and the sound velocity in the nm^{-1} wavenumber and meV energy regimes was determined. Compared with the corresponding values in the hydrodynamic limit, the sound velocity in the nm^{-1} regime was faster, and the positive dispersion of the longitudinal modulus was stronger in liquids composed of ring structures (cyclohexane and 1,4-dioxane) than in those of linear chain structures (n-hexane and ethylene glycol dimethyl ether). Molecular dynamics simulation of n-hexane and cyclohexane was also performed. The difference in the positive dispersion of the longitudinal modulus was reproduced by simulation, and it was elucidated by the difference in the longitudinal modulus in the $q = 0$ limit and the THz frequency regime. The excess part of the longitudinal modulus from the hydrodynamic limit was further divided into various contributions, and the smaller excess modulus of n-hexane was mainly ascribed to two reasons. The first one is that the shear modulus of n-hexane is smaller in the THz regime, and the second one is that the positive dispersion of the bulk modulus due to the vibrational energy relaxation is weaker. The second mechanism was further interpreted in terms of the fast vibrational energy relaxation of intramolecular modes associated with the chain deformation of n-hexane.

Published under an exclusive license by AIP Publishing. https://doi.org/10.1063/5.0107387

I. INTRODUCTION

Shear viscosity is a transport coefficient that governs the macroscopic flow of liquids, defined as the proportionality coefficient between the shear stress and the shear rate. It is a measure of the ease to flow the liquid, that is, the flow of liquids with high viscosity is accompanied by a large pressure drop. In addition, microscopic dynamic processes, such as the diffusivity and reaction rate of a solute dissolved in a solvent, are often related to the macroscopic shear viscosity of solvents. A solute is less diffusive in solvents of high viscosity, and its chemical reaction would be retarded there. It is thus both interesting and important to understand microscopic mechanisms that determine the macroscopic shear viscosity of organic liquids.

Shear viscosity is described in terms of the time correlation function of the shear stress integrated over the whole time according to the Kubo–Green theory,[1] and it is approximately given by the product of the shear modulus in the high-frequency limit and the relaxation time.[2] The latter reflects the dynamics of microscopic modes that determine the shear viscosity. Information on the relaxation time can be obtained experimentally by measuring the frequency dependence of the shear viscosity through the application of the oscillatory shear flow to sample liquids instead of the steady flow. Knowing the relaxation time, it can be compared with those of other experiments, such as quasi-elastic neutron scattering, to estimate the dynamic modes that exhibit similar relaxation times.[3–6]

The measurement of frequency-dependent shear viscosity is possible with commercial mechanical rheometers up to the kHz regime, and it is routinely applied to soft materials, such as polymer and surfactant systems. Measurement in the MHz regime is possible by means of a quartz crystal microbalance with dissipation

(QCM-D)-based method,[7–10] which has revealed shear relaxation of various viscous liquids, including room-temperature ionic liquids.[11] We have recently proposed an experimental method that extends the applicable frequency range of the QCM-D-based measurement up to 3 GHz.[12] A novel method based on the mechanical resonance of nanoparticles was also proposed to measure the shear viscosity around several tens of GHz.[13,14] However, the shear relaxation of low-viscosity organic solvents is expected to occur in the THz frequency regime, where no experimental method has yet been proposed.

An experimental method closely related to the shear relaxation is ultrasonic spectroscopy, in which the velocity or the attenuation coefficient of ultrasound is measured as the function of frequency.[15] A simple hydrodynamic equation predicts that the sound velocity is independent of frequency and the attenuation coefficient is proportional to the squared frequency, and the relaxation process appears as the deviation from these hydrodynamic predictions. Ultrasonic spectroscopy in the kHz to MHz regime is usually performed with electric methods. Brillouin spectroscopy using visible lasers is available in the GHz regime. Owing to the development of dedicated beamlines at synchrotron facilities, it is now possible to measure sound waves in the THz regime using inelastic x-ray scattering (IXS) spectroscopy.[16,17] The measurement of the sound wave in the THz regime has traditionally been performed using inelastic neutron scattering, and it was applied to various liquids, including liquid metals and water.[18] However, the inelastic neutron scattering suffers from the kinematic limitation and the large incoherent scattering of protons, and the development of IXS enabled Brillouin spectroscopy in the THz regime without such limitations.

The viscosity directly determined by ultrasonic spectroscopy is the longitudinal viscosity, which is given by the linear combination of the contributions of shear and volume viscosities. Volume viscosity is defined as the response of the isotropic pressure to the rate of the adiabatic isotropic compression, and it is given by the time correlation function of the adiabatic pressure fluctuation. It can thus reflect microscopic processes involving enthalpy or volume changes, such as isomeric reaction and vibrational energy relaxation.[15] Provided that these processes do not appear in the frequency dependence of shear viscosity, the appearance of a relaxation mode in the longitudinal viscosity never means the presence of the shear relaxation, and the information on the frequency-dependent volume viscosity is indispensable to probe the shear relaxation through ultrasonic spectroscopy.

Another point to be noted in the analysis of an IXS spectrum is the wavenumber dependence of material properties. Because the wavenumber of the sound in the THz frequency regime is close to the reciprocal size of molecules, variation in mechanical properties, such as storage and loss moduli, with the wavenumber can also be a reason for the dispersion of the sound velocity.

IXS spectroscopy has been applied to various popular organic liquids, including benzene, acetone, carbon tetrachloride, and others, and demonstrated the presence of "fast sound," that is, the sound velocity in the nm^{-1} wavenumber regime is higher than that in the hydrodynamic limit.[18–22] As the dispersion of the sound velocity in this wavenumber regime is usually ascribed to the viscoelastic relaxation, the fast sound of these solvents may contain information of relaxation processes that determine their viscosity. In the analysis

of the fast sound, there are some shortages on both the experimental and theoretical sides. On the experimental side, the choice of the studied systems was not systematic; hence, it was difficult to relate the difference in the fast sound to the molecular structure and the intermolecular interaction. On the theoretical side, it was unclear how much the wavenumber dependence of various properties should be taken into account to understand the sound dispersion in the nm^{-1} regime and, furthermore, the wavenumber dependence of what property should be included. In addition, although various physicochemical processes, including vibrational energy relaxation, contribute to the volume viscosity and the bulk modulus, there is, to the best of our knowledge, no theoretical formalism to extract these contributions.

In this work, we perform IXS experiments on four organic liquids: n-hexane, cyclohexane, ethylene glycol dimethyl ether (EGDME), and 1,4-dioxane. All four liquids are used as common organic solvents, and their molecular sizes are similar. A comparison between n-hexane and cyclohexane and between EGDME and 1,4-dioxane reveals differences in the molecular structures—a linear chain or a ring. The effects of the introduction of ether groups are inferred from the difference between n-hexane and EGDME and that between cyclohexane and 1,4-dioxane. The experimental results in this work show that the effects of the introduction of ether groups are small, whereas the formation of a ring structure significantly increases the degree of the positive dispersion of the longitudinal modulus. In order to investigate the origin of the latter, in this work, we perform molecular dynamics (MD) simulation of liquid n-hexane and cyclohexane. The difference in the positive dispersion is well reproduced by MD simulation.

In earlier work done by one of the authors (Yamaguchi), MD simulation of Lennard-Jones (LJ) fluids and model cyclohexane was performed;[23] the results showed that the positive sound dispersion of up to ~2 nm^{-1} can be elucidated quantitatively by the relaxation of the longitudinal viscosity in the $q = 0$ limit, where q stands for the wavenumber. After dividing the longitudinal viscosity into shear and volume viscosities, the work also proposed a theoretical formalism to extract the contribution of vibrational energy relaxation to the volume viscosity based on the projection operator formalism.
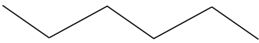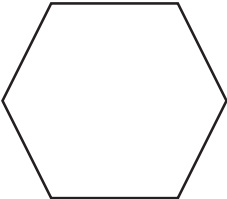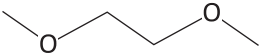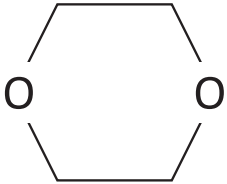
Based on the results of the earlier work, we now, in this work, analyze the difference in sound dispersions of n-hexane and cyclohexane in terms of the relaxation of longitudinal viscosity in the $q = 0$ limit. After the division into the contributions of shear and volume viscosities, the contribution of the vibrational energy relaxation to the volume viscosity is also calculated, and its contribution to the difference in the sound dispersion of the two liquids is separated. We then discuss what the difference in the positive dispersion of the longitudinal modulus of these liquids tells us about the mechanisms of their shear viscosity.

II. METHODS

A. Samples

Four sample liquids, n-hexane, cyclohexane, EGDME, and 1,4-dioxane (anhydrous grade, for organic synthesis), were purchased from Kanto Chemical Co. and used as received. The physical properties of the samples at 298 K are summarized in Table I.

TABLE I. The molecular structure, density (ρ_m), shear viscosity (η_s), and hydrodynamic sound velocity (c_0) of the sample liquids at 298 K.

Name	Molecular structure	ρ_m (g/cm^3)	η_s (mPa s)	c_0 (m/s)
n-hexane		0.6550[a]	0.292[a]	1086[b]
Cyclohexane		0.7738[c]	0.898[d]	1255[c]
EGDME		0.8611[e]	0.417[e]	1146[e]
1,4-dioxane		1.0292[f]	1.180[f]	1345[f]

[a]Reference 24.
[b]Reference 25.
[c]Reference 26.
[d]Reference 27.
[e]Reference 28.
[f]Reference 29.

B. IXS experiments

The IXS experiments were carried out at BL43LXU of SPring-8 using a high resolution IXS spectrometer.[30–32] A beam of ~2×10^{10} photons s^{-1} in a 0.8 meV bandwidth was obtained from an undulator source through a cryogenically cooled Si(111) double crystal monochromator followed by a Si(11 11 11) backscattering crystal. The radiation scattered from the sample was analyzed using 28 spherical Si analyzers on a 10 m detector arm, and the IXS signals were collected using low-background CdZnTe detectors. The total energy resolution was determined by measuring the scattering from Tempax glass and deconvolving the phonon response,[33] giving 1.3–1.8 meV full width at half maximum (FWHM), depending on the analyzer crystal. The wavenumber resolution was determined by 40×85 mm^2 slits, 1 m in front of the analyzer crystals, to be about 0.6 nm^{-1} full width.

Liquid samples were contained in a thin-walled (250 μm) sapphire cell machined out of a single crystal material[22] (sample thickness ~1 mm), which is a slight modification of the Tamura-type cell.[34] All measurements were carried out at room temperature. To avoid evaporation of the sample, the sample reservoir was sealed with a perfluoroelastomer O ring (Kalrez®) and stainless-steel parts. The sample and the sapphire cell were placed in a vessel[35] equipped with sapphire windows (thickness 0.40 mm). The vessel was filled with He gas to avoid strong x-ray scattering by air. The background from the sapphire cell was measured and found to be negligible compared to the signal over the Q, E range explored in the present experiment. A typical energy scan over ±15 meV took ~1 h. Two scans were performed to improve the counting statistics.

C. Small-angle x-ray scattering experiments

Small-angle x-ray scattering (SAXS) measurements were performed with a Nano-Viewer small-angle x-ray diffractometer (Rigaku) using Cu Kα radiation (λ = 0.154 18 nm). All measurements were performed at room temperature. The range of the measured scattering vector, q, was 1.5–17.0 nm^{-1}, where q is related to the scattering angle, 2θ, as $q = (4\pi/\lambda)\sin\theta$. The scattering vector was calibrated by the measurement of silver behenate powder. The sample solution was sealed into a borosilicate glass capillary (diameter 1.5 mm, wall thickness 10 μm). The scattering intensity of the solution was obtained by subtracting the scattering intensity from the capillary after the absorption correction.

D. MD simulation

MD simulation of liquid n-hexane and cyclohexane was performed using the GROMACS software package.[36] The force field used was the Optimized potentials for liquid simulations-All atom (OPLS-AA) model.[37] Simulation was performed under the constant volume and constant temperature (NVT) ensemble; the temperature was fixed to be 298.15 K using a Nosé–Hoover thermostat.[38] The time constant of the thermostat was 100 ps, which was set to be sufficiently long to avoid a possible artifact in the dynamics of adiabatic pressure fluctuation used for the calculation of

volume viscosity. The size of the cubic cell used for simulation was 6.022 89 nm, and the periodic boundary conditions were applied to the cell. The numbers of molecules in a cell were 1000 for *n*-hexane and 1210 for cyclohexane, which reproduce the experimental densities at the ambient pressure.[24,26,27] The lengths of bonds involving a hydrogen atom were fixed using the LINCS algorithm,[39] and other intramolecular degrees of freedom were treated as flexible. The long-range part of the electrostatic interaction was calculated using the particle mesh Ewald method,[40] and the short-range part, together with the LJ interaction, was cut off at 1.2 nm. The equation of motion was integrated by means of the leapfrog algorithm with the time step of 1 fs. The length of the production run was 100 ns, preceded by the equilibration run of 100 ns length.

III. RESULTS AND DISCUSSION

A. Small-angle x-ray scattering experiments

The SAXS profiles of the four liquids are shown in Fig. 1. A strong peak is observed in all the profiles between 12 and 14 nm^{-1}, as is the case for many molecular liquids. Roughly speaking, the character of the SAXS profile depends on whether the molecule possesses a ring or a chain shape. The profiles of liquids with ring structures (cyclohexane and 1,4-dioxane) exhibit a strong and sharp peak, whereas those of liquids with chain structures (*n*-hexane and EGDME) exhibit a broad peak.

B. IXS experiments

The IXS spectra of the four sample liquids at $q = 3.71$ nm^{-1} are plotted as a function of the energy transfer, E, in Fig. 2, as examples. The energy transfer of $E = 1$ meV corresponds to the shift of the angular frequency of 1.52 ps^{-1}. All four spectra have a central peak at $E = 0$ and shoulders at $E \sim \pm 4$ meV. The triple-peak structure is common to the Rayleigh–Brillouin spectrum—a typical spectral shape of the optical light scattering of liquids. At long wavelengths, the central Rayleigh peak is assigned to the heat diffusion and the Brillouin doublet to the longitudinal sound wave. Comparing the spectra of the four liquids, it is noted that the shoulders of cyclohexane and 1,4-dioxane appear more clearly than those of *n*-hexane and EGDME.
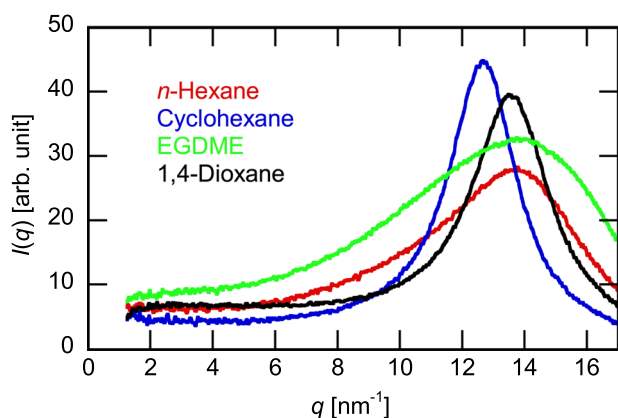

FIG. 1. Experimental SAXS profiles of *n*-hexane (red), cyclohexane (blue), EGDME (green), and 1,4-dioxane (black).
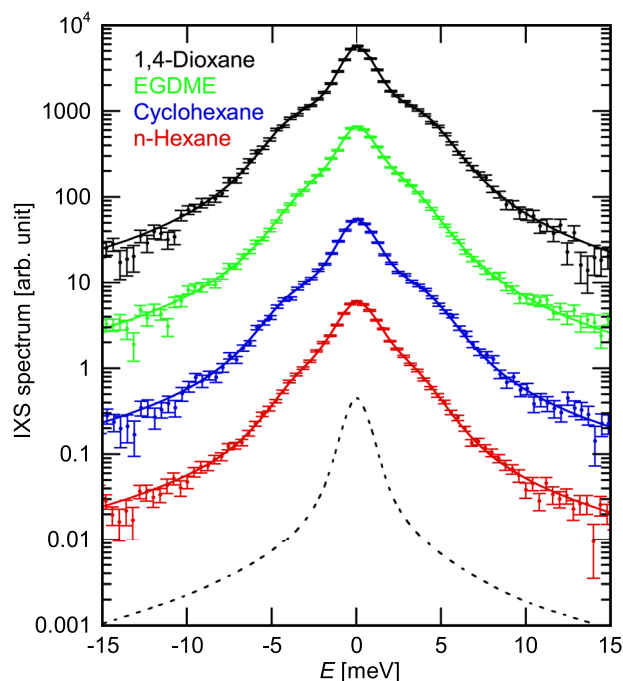

FIG. 2. IXS spectra of *n*-hexane (red), cyclohexane (blue), EGDME (green), and 1,4-dioxane (black) at $q = 3.71$ nm^{-1}. Experimental spectra are shown with filled circles, and the fitting curves using Eq. (1) are drawn with solid curves. The longitudinal axis is drawn on a log scale, and the spectra of the four samples are vertically shifted to enhance visibility. The resolution function is indicated as the lowest dotted curve.

The IXS spectra of the four samples at all the wavenumbers are approximated by employing the model function for the dynamic structure factor as[41]

$$S(q,E) = I_0 \left[\frac{w_1}{E^2 + w_1^2} + \frac{2a_2 w_2 \Omega^2}{\left(E^2 - \Omega^2\right)^2 + 4w_2^2 E^2} + \frac{w_1(\Omega^2 - E^2)}{\left(E^2 - \Omega^2\right)^2 + 4w_2^2 E^2} \right]. \quad (1)$$

The first and the second terms describe the Rayleigh peak and the Brillouin doublet. Although the third term is usually neglected in the analysis of optical Brillouin spectrum, the recent work has demonstrated that the inclusion of the third term gives a better description of the IXS spectrum of liquid water.[41] The fitting is performed by, first, multiplying by a Bose factor for a detailed balance and, second, convolving the resolution function. The temperature for the calculation was taken to be 300 K. The five quantities I_0, w_1, a_2, Ω, and w_2 are treated as free-fitting parameters. Examples of the fitting are demonstrated in Fig. 2 as the solid curves—there is good agreement with the experimental spectra.

The four fitting parameters a_2, w_1, Ω, and w_2 of the four liquids are plotted as a function of wavenumber in Fig. 3. The parameter I_0 is omitted here because it is scaled with the total intensity. The relative amplitude of the Brillouin doublet to the central Rayleigh peak, a_2, is shown in Figs. 3(a) and 3(b). The relative amplitude is a
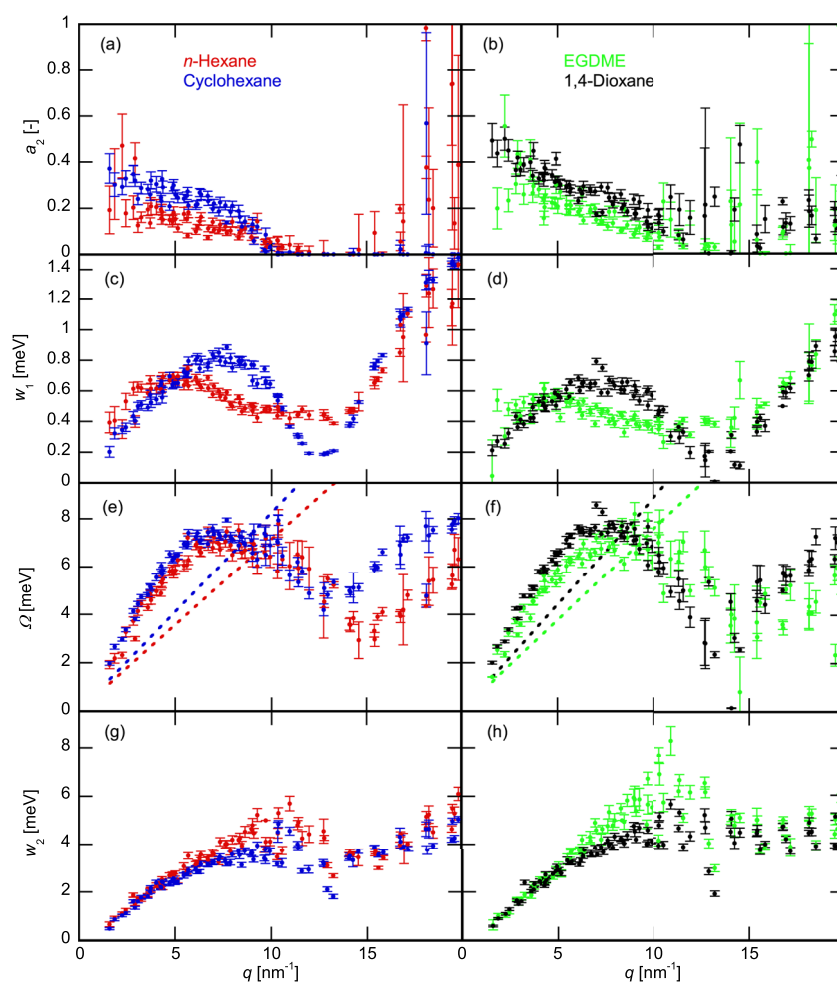
FIG. 3. Fitting parameters (a) and (b) a_2, (c) and (d) w_1, (e) and (f) Ω, and (g) and (h) w_2. The results of n-hexane, cyclohexane, EGDME, and 1,4-dioxane are shown with the red, blue, green, and black symbols, respectively. The dotted lines in (e) and (f) indicate the expectation from the hydrodynamic sound velocities.

decreasing function of q at $q < 10$ nm^{-1}, and it approaches zero near $q = 10$ nm^{-1}. The value of a_2 scatters at higher q, with accompanying large fitting errors. The reason for the scatter and the large error is because the separation of the IXS spectra into the Rayleigh and Brillouin ones works poorly in this wavenumber region. Therefore, we limit the discussion on the acoustic properties from the fitting parameters at $q < 10$ nm^{-1}.

The width of the central peak, w_1, shown in Figs. 3(c) and 3(d), is a nonmonotonic function of q. It first increases with q from $q = 0$, and the q dependence is inverted at the intermediate q region, whereafter it increases with q again at higher q. Compared with the static structure factor shown in Fig. 1, the minimum wavenumber of the minimum width is close to the peak of the static structure factor in all four liquids. The slowing down of the collective density dynamics around the peak of the static structure factor is well known as "de Gennes narrowing,"[1] and the nonmonotonic wavenumber dependence of w_1 [shown in Figs. 3(c) and 3(d)] can be understood as the manifestation of the de Gennes narrowing. Comparing the widths of the four liquids, their q dependences appear to be related to the molecular shape, as is the case of the static structure factor. The

liquids composed of ring molecules, cyclohexane and 1,4-dioxane, exhibit a sharp and strong de Gennes narrowing, corresponding to sharper peaks in the static structure factor. The narrowing begins at lower q in liquids of chain molecules (n-hexane and EGDME); the degree of the narrowing is rather weak, consistent with the broad peak of the static structure factor in Fig. 1.

The center of the Brillouin peak, Ω, plotted in Figs. 3(e) and 3(f), is related to the wavenumber-dependent sound velocity, $c(q)$, as

$$c(q) = \frac{\Omega}{\hbar q}. \qquad (2)$$

Here, $\hbar = h/2\pi$ is the reduced Planck constant. In Figs. 3(e) and 3(f), the dotted straight line shows the expectation from the relation as $c(q) = c_0$, where c_0 denotes the sound velocity in the hydrodynamic limit, shown in Table I. The values of Ω in Figs. 3(e) and 3(f) are larger than the hydrodynamic expectation at $q < 7$ nm^{-1}, which is common to other liquids. The upward deviation from the hydrodynamic value means that the sound velocity in this

wavenumber regime is larger than the hydrodynamic one; that is, fast sound is observed in these four liquids. The frequencies of the acoustic oscillation of liquids composed of ring molecules, cyclohexane and 1,4-dioxane, are larger than those of chain molecules, n-hexane and EGDME, as is expected from Fig. 2. However, since the hydrodynamic sound velocities of the former are also larger than those of the latter, a detailed analysis of the difference is necessary.

The width of the Brillouin doublet, w_2, shown in Figs. 3(g) and 3(h), increases with increasing q at $q < 10$ nm^{-1} in all four liquids. The hydrodynamic theory predicts that w_2 is proportional to q^2, and the proportionality coefficient is given in terms of the longitudinal viscosity and the heat diffusivity. However, the q dependence of w_2 [shown in Figs. 3(g) and 3(h)] is weaker than q^2 in all the liquids. As the frequency of the acoustic oscillation, $\Omega/\hbar$, is expected to be comparable with or higher than the viscoelastic relaxation frequency, the longitudinal viscosity would be a decreasing function of frequency, which would explain the deviation of w_2 from the hydrodynamic q^2 dependence.

The wavenumber-dependent sound velocity, $c(q)$, is calculated from the frequency of the Brillouin doublet, Ω, using Eq. (2) and plotted as a function of q in Figs. 4(a) and 4(b). The hydrodynamic sound velocities, c_0, are also indicated by the horizontal lines for comparison. In all the liquids, $c(q)$ at $q = 3$–4 nm^{-1} is several tens of percent larger than c_0, and it decreases with increasing q in the higher q region.

The excess longitudinal modulus, $\Delta G'_L$, is defined here from $c(q)$ as

$$\Delta G'_L \equiv \rho_m\left[c^2(q) - c_0^2\right], \tag{3}$$

where ρ_m denotes the mass density. When the q dependence of material properties is wholly negligible, $\Delta G'_L(q)$ is related to the imaginary part of the frequency-dependent longitudinal viscosity, $\eta''_L(\omega)$, as

$$\Delta G'_L(q) = \frac{\Omega(q)}{\hbar} \eta''_L\left(\frac{\Omega(q)}{\hbar}\right). \tag{4}$$

The calculated values of $\Delta G'_L(q)$ are shown in Figs. 4(c) and 4(d); they are also decreasing functions of q at $q > 4$ nm^{-1}. Comparing the values of the four liquids, the liquids of ring molecules exhibit higher modulus than those of chain molecules, and the liquids with similar structures show similar modulus, irrespective of the presence of ether groups. Although the values of $\Delta G'_L(q)$ of ethers appear slightly larger than those of hydrocarbons of the corresponding structures, the difference is much smaller than the difference between the chain and the ring species. Therefore, the molecular structure has a stronger effect on the fast sound than the electrostatic interaction induced by the polar ether groups.

Earlier MD simulation work carried out by one of the authors (Yamaguchi) suggested that the sound dispersion of two models of cyclohexane up to $q = 2$ nm^{-1} is fully ascribed to the viscoelastic relaxation in the $q = 0$ limit and that the wavenumber dependence of the heat capacity ratio should be taken into account for the quantitative description of sound dispersion at higher q.[23] Based on this result, we consider that the larger values of $\Delta G'_L(q)$ of liquids of ring molecules than those of chain molecules around $q = 3$–4 nm^{-1} can be ascribed to the difference in the longitudinal viscoelastic relaxation, at least qualitatively, although an explanation of the higher q behaviors would require information on the q dependence of material properties.

C. MD simulation

The x-ray static structure factors of n-hexane and cyclohexane are calculated from MD simulation and plotted in Fig. 5. On calculating both the x-ray static structure factors and the intermediate scattering functions, the scattering length of each atom is assumed proportional to the atomic number; the wavenumber dependence of the form factor is neglected in this work. The structure factors from MD simulation (Fig. 5) capture the characteristics of the experimental ones (Fig. 1). The structure factor of cyclohexane shows a strong and sharp peak, whereas the peak of n-hexane is broad and exhibits a tail down to lower wavenumbers. The peak wavenumber
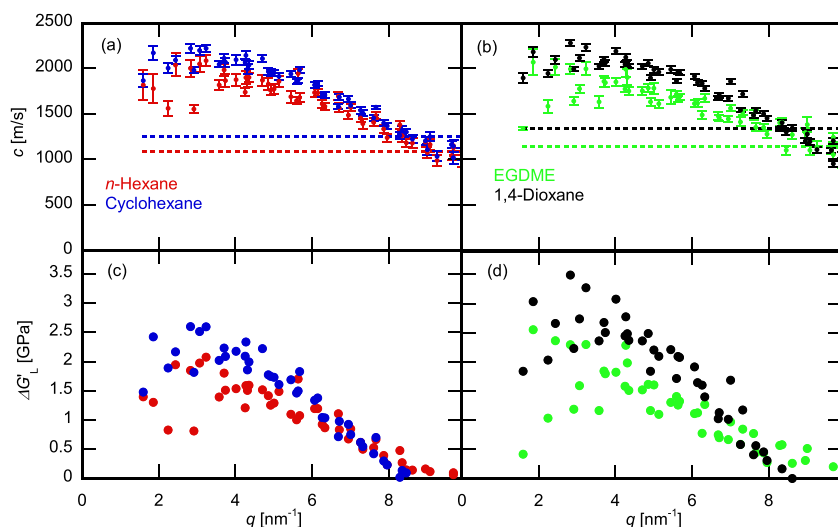

FIG. 4. (a) and (b) $c(q)$. (c) and (d) $\Delta G'_L(q)$ of n-hexane (red), cyclohexane (blue), EGDME (green), and 1,4-dioxane (black). The error bars are omitted in (c) and (d) for visibility.
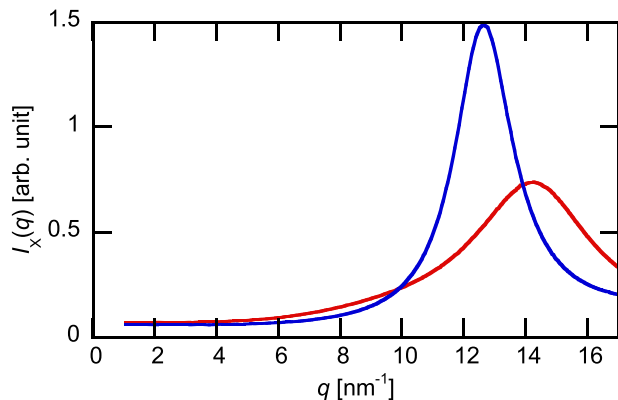
FIG. 5. X-ray static structure factors of *n*-hexane (red) and cyclohexane (blue) calculated by MD simulation.

of *n*-hexane is higher than that of cyclohexane; their peak positions are close to the corresponding experimental ones in Fig. 1.

The intermediate scattering function is calculated from MD simulation at wavenumbers $q = nq_{min}$, where n is an integer and q_{min} is the minimum wavenumber of a cubic cell of size L, $q_{min} \equiv 2\pi/L$. Provided that the time-domain version of the experimental model function, Eq. (1), is given by

$$\frac{I_{model}(q,t)}{\tilde{\chi}(q)} = (1 - a_P(q))\left[e^{-k_T(q)t} + \frac{k_T(q)}{\omega'_P(q)}e^{-k_P(q)t}\sin\omega'_P(q)t\right]$$
$$+ a_P(q)e^{-k_P(q)t}\left[\cos\omega'_P(q)t + \frac{k_P(q)}{\omega'_P(q)}\sin\omega'_P(q)t\right],$$

(5)

we first tried to fit the intermediate scattering function from simulation, $I_{MD}(q,t)$, by $I_{model}(q,t)$. However, we found that $I_{model}(q,t)$ cannot well reproduce $I_{MD}(q,t)$ in the whole-time region, as is demonstrated in Fig. S1 of the supplementary material. Therefore, the fitting procedure was modified as follows: keeping the correspondence with the fitting of experimental spectra.

The experimental spectrum is described as the convolution of the model function, Eq. (1), and the resolution function due to the finite spectral resolution. The convolution in the frequency domain corresponds to the multiplication of the window function, $w(t)$, in the time domain, and $w(t)$ is given by the Fourier transformation of the resolution function. The fitting was thus performed to minimize the squared error between $w(t)I_{MD}(q,t)$ and $w(t)I_{model}(q,t)$, and this fitting procedure is equivalent to the weighted least-squares fitting with the weighting factor of $w^2(t)$. The Gaussian functional form of the window function is assumed for simplicity as

$$w(t) = \exp\left(-\frac{t^2}{2\tau_w^2}\right),$$

(6)

and the time constant τ_w was determined to be 1 ps as a typical value from the Gaussian fitting of the resolution functions. The examples of the fitting with and without the window function are compared in Fig. S1 of the supplementary material. After the introduction of the window function, the intermediate scattering functions from MD

simulation are reproduced well by the fitting function in the short-time region ($t < 2$ ps). The five parameters in Eq. (5), $\tilde{\chi}(q)$, $a_P(q)$, $k_T(q)$, $\omega'_P(q)$, and $k_P(q)$, were optimized as free-fitting parameters, and the wavenumber-dependent sound velocity, $c(q)$, is evaluated as

$$c(q) = \frac{\sqrt{\omega'^2_P(q) + k^2_P(q)}}{q}.$$

(7)

The wavenumber-dependent sound velocity from MD simulation is compared with that from experiments shown in Fig. 6. The results of MD simulation agree well with those of experiments, suggesting that the mechanism of the difference in the sound dispersions of both liquids can be extracted from the analysis of present simulation.

Because the acoustic wave in the IXS spectrum occurs in the THz frequency and the nm^{-1} wavenumber regimes, the differences in both the frequency and the wavenumber can be a reason for the deviation of the sound velocity in the IXS experiment from the hydrodynamic one, in principle. However, one of the authors (Yamaguchi) showed that, in the case of a model cyclohexane, the effect of frequency is dominant up to $q = 2$ nm^{-1} and that the fast sound is mainly ascribed to the longitudinal viscoelasticity in the $q = 0$ limit.[23]

Based on the results of the earlier work,[23] the frequency-dependent excess longitudinal modulus, denoted as $\Delta G'_L(\omega)$, was evaluated in the following way. According to Kubo–Green theory, the frequency-dependent complex shear viscosity, $\eta_s(\omega)$, is given by the time correlation function of the shear stress, P_{xy}, as[1]

$$\eta_s(\omega) = \frac{V}{k_B T}\int_0^\infty dt\, e^{-i\omega t}\langle P_{xy}(0)P_{xy}(t)\rangle,$$

(8)

where V, k_B, and T denote the volume of the system, the Boltzmann constant, and the absolute temperature, respectively. The frequency-dependent shear modulus, $G_s(\omega)$, is then given by the imaginary part of $\eta_s(\omega)$ as

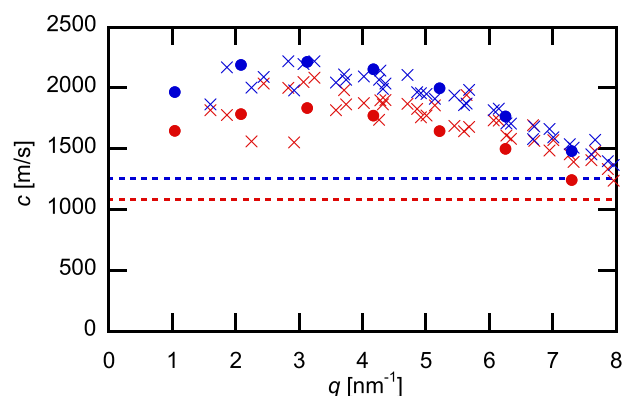$$G'_s(\omega) = \omega\eta''_s(\omega).$$

(9)

FIG. 6. Wavenumber-dependent sound velocity from MD simulation (filled circles) and experiments (crosses). The horizontal lines indicate the sound velocity in the hydrodynamic limit shown in Table I. The results of *n*-hexane and cyclohexane are shown with the red and the blue symbols, respectively.

The frequency-dependent complex volume viscosity, $\eta_v(\omega)$, is similarly related to the adiabatic pressure fluctuation, $\delta P'$, as[42–44]

$$\eta_v(\omega) = \frac{V}{k_B T} \int_0^\infty dt\, e^{-i\omega t} \langle \delta P'(0) \delta P'(t) \rangle. \qquad (10)$$

In the NVT ensemble, $\delta P'$ is described as the component of the pressure fluctuation, δP, that is orthogonal to the total energy fluctuation, δE, as

$$\delta P'(t) \equiv \delta P(t) - \frac{\langle \delta P \delta E \rangle}{\langle |\delta E|^2 \rangle} \delta E(t). \qquad (11)$$

The frequency-dependent excess volume modulus, $\Delta K'(\omega)$, is related to the imaginary part of $\eta_v(\omega)$ as

$$\Delta K'(\omega) = \omega \eta_v''(\omega), \qquad (12)$$

and $\Delta G_L'(\omega)$ is described as the linear combination of $G_s'(\omega)$ and $\Delta K'(\omega)$ as

$$\Delta G_L'(\omega) = \Delta K'(\omega) + \frac{4}{3} G_s'(\omega). \qquad (13)$$

The excess longitudinal moduli, $\Delta G_L'(\omega)$, of both liquids calculated based on the Kubo–Green theory are plotted as a function of angular frequency, ω, in Figs. 7(a) and 7(b) (green curves). The frequency range relevant to the sound dispersion observed in the nm^{-1} wavenumber range is $\sim 1 < \omega < 10$ ps^{-1}. The excess longitudinal modulus of cyclohexane is larger than that of n-hexane, as is estimated experimentally from the sound dispersion in the nm^{-1} wavenumber regime. The larger degree of the positive dispersion of the longitudinal modulus of cyclohexane than that of n-hexane is thus ascribed to the larger excess longitudinal modulus in the $q = 0$ limit.

The contributions of the excess volume modulus, $\Delta K'(\omega)$, and those of the shear modulus, $\frac{4}{3} G_s'(\omega)$, are also shown in Figs. 7(a) and 7(b). In both liquids, the relaxation of the former is slower than that of the latter, which suggests that these two moduli are governed by the different microscopic dynamic modes. Upon comparing the corresponding functions of cyclohexane and n-hexane, both terms contribute to the larger longitudinal modulus of cyclohexane—the contribution of $\Delta K'(\omega)$ is a little larger than that of $\frac{4}{3} G_s'(\omega)$.

The positive sound dispersion in the GHz frequency regime has been reported experimentally in many organic liquids, including cyclohexane, and it has been assigned to the vibrational energy relaxation.[45] Although, to the best of our knowledge, the corresponding positive dispersion has not been reported for n-hexane, the positive sound dispersion may also exist in n-hexane. As the intramolecular vibrational modes other than the C–H stretching ones are included in present MD simulation, the vibrational energy relaxation can also contribute to the excess volume modulus obtained by simulation.

In an earlier study, one of us (Yamaguchi) proposed a theoretical formalism to extract the contribution of the vibrational energy relaxation to the frequency-dependent complex volume viscosity, $\eta_v(\omega)$.[23] The fluctuation of the total energy of the system, $\delta E(t)$, is first divided into the rigid part, $\delta E_1(t)$, and the intramolecular vibrational energy, $\delta E_2(t)$. The definition of the division in this work is the same as that in the earlier work.[23] The linear correlations of $\delta E_1(t)$ and $\delta E_2(t)$ with $\delta E(t)$ are then projected out to define $\delta E_1'(t)$ and $\delta E_2'(t)$, as is performed in Eq. (8) on δP. The rigid and vibrational energy relaxation parts of the complex volume viscosity, denoted as $\eta_{v1}(\omega)$ and $\eta_{v2}(\omega)$, respectively, are given by

$$\eta_{v2}(\omega) = \frac{V \left[\int_0^\infty dt\, e^{-i\omega t} \langle \delta P'(0) \delta E_{2'}(t) \rangle \right]^2}{k_B T \int_0^\infty dt\, e^{-i\omega t} \langle \delta E_{2'}(0) \delta E_{2'}(t) \rangle}, \qquad (14)$$

$$\eta_{v1}(\omega) = \eta_v(\omega) - \eta_{v2}(\omega). \qquad (15)$$

It was demonstrated in the earlier study that $\eta_{v1}(\omega)$ obtained above by subtracting the contribution of the intramolecular vibrational mode is close to the complex volume viscosity calculated by MD simulation of the rigid intramolecular structure.[23]
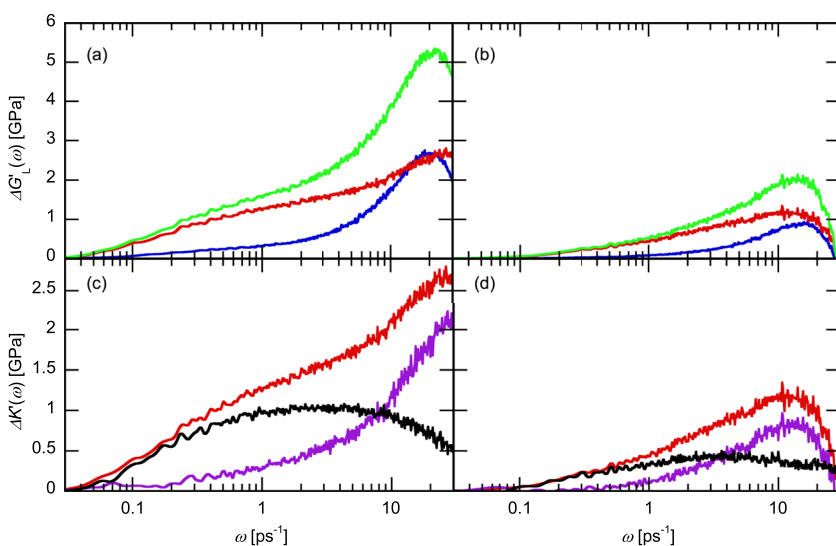

FIG. 7. (a) and (b) The excess longitudinal moduli (green) are divided into the contributions of shear (blue) and excess volume (red) moduli. (c) and (d) The excess volume moduli (red) are further divided into the contributions of the vibrational energy relaxation (black) and rigid (purple) parts. The results of cyclohexane are shown in (a) and (c), whereas those of n-hexane are shown in (b) and (d).

The division of the excess volume modulus, $\Delta K'(\omega)$, is then defined as

$$\Delta K_1'(\omega) \equiv \omega \eta_{v1}''(\omega), \tag{16}$$

$$\Delta K_2'(\omega) \equiv \omega \eta_{v2}''(\omega). \tag{17}$$

The numerical results of the division are shown in Figs. 7(c) and 7(d). In both liquids, the relaxation of $\Delta K_2'(\omega)$ is slower than that of $\Delta K_1'(\omega)$, and the frequency dependence of the rigid part is comparable with that of the shear modulus in Figs. 7(a) and 7(b). The slower relaxation of $\Delta K'(\omega)$ than that of $G_s'(\omega)$ is thus ascribed to the contribution of the slow vibrational energy relaxation, and the dynamics reflected in the rigid part, $\Delta K_1'(\omega)$, is expected to be the same as that giving the shear modulus. Comparing the corresponding functions of the two liquids, both $\Delta K_1'(\omega)$ and $\Delta K_2'(\omega)$ are larger in cyclohexane than in n-hexane, but the difference in the former is much larger than that in the latter. Therefore, the larger excess volume modulus of cyclohexane is mainly ascribed to the contribution of the vibrational energy relaxation.

The relaxation amplitude of the sound dispersion due to the vibrational energy relaxation is related theoretically to the vibrational heat capacity. In classical MD simulation performed in this work, the vibrational heat capacity per an intramolecular vibrational mode is k_B, irrespective of its vibrational frequency, and the total vibrational heat capacity is proportional to the number of vibrational modes. As the numbers of atoms per molecule in n-hexane and cyclohexane are similar, their vibrational heat capacity should be similar, which appears to contradict the larger relaxation amplitude of $\Delta K_2'(\omega)$ of cyclohexane than that of n-hexane.

The autocorrelation functions of $\delta E_2'(t)$ of both liquids are shown in Fig. 8 to analyze the difference in the relaxation amplitude of $\Delta K_2'(\omega)$. The correlation functions are normalized to the numbers of molecules in the systems, N. The relaxation of the autocorrelation functions is bimodal in both liquids, consisting of the fast sub-ps and slow ps components. The initial values of both liquids are close to each other, which is consistent with the similar vibrational heat capacity in classical MD simulation, because the equilibrium fluctuation of energy is related to the heat capacity.
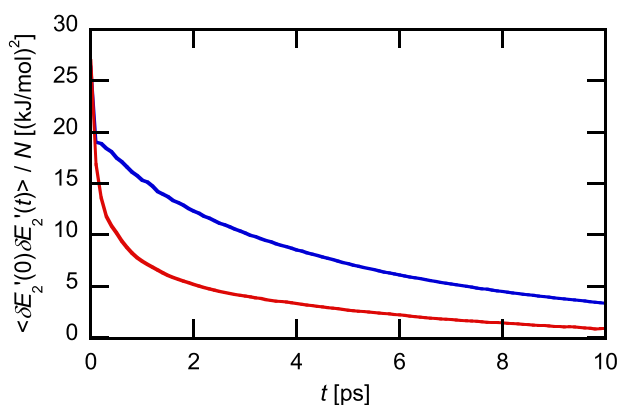

FIG. 8. Autocorrelation functions of $\delta E_2'(t)$ of n-hexane (red) and cyclohexane (blue). The two curves overlap with each other at $t < 0.1$ ps.

The large difference between both liquids exists in the amplitude of the slow component. The vibrational energy relaxation gives the excess longitudinal modulus when the vibrational energy relaxation is slower than the acoustic oscillation. The longitudinal sound increases the translational and rotational energies of molecules during the adiabatic compression. When the vibrational energy relaxation is slower than the period of the acoustic oscillation, the translational and rotational energies are transferred into the intramolecular vibrational modes, and the increase in the pressure through the decrease in the translational and the rotational temperatures is reduced. In contrast, such a mechanism does not work when the vibrational energy relaxation is slow, and the longitudinal modulus becomes larger than the hydrodynamic one. Provided that the angular frequency of the acoustic oscillation is 1–10 ps^{-1} in the nm^{-1} wavenumber regime, only the slow part of the relaxation of $\delta E_2'(t)$ is expected to contribute to the excess modulus. Therefore, the smaller $\Delta K_2'(\omega)$ in n-hexane can be ascribed to the smaller amplitude of the slow component of the relaxation of $\delta E_2'(t)$ in Fig. 8.

The next question to be addressed is the reason for the difference in the amplitude of the slow component, which we consider is related to the difference in the molecular flexibility. Many intramolecular vibrational modes of n-hexane involve chain deformation. The vibrational energy relaxation of such modes is expected to be fast because they are strongly coupled to the translational and rotational dynamics of surrounding molecules, and these modes would contribute to the fast dynamics of $\delta E_2'(t)$. In contrast, the intramolecular vibrational modes of cyclohexane are rather isolated from the dynamics of the surrounding molecules due to its rigid structure, which explains the relatively small amplitude of the fast component.

We should comment here on the effects of possible artifacts of classical MD simulation because classical approximation of intramolecular vibration overestimates the vibrational heat capacity. One may thus consider that the discussion based on the difference in the vibrational energy relaxation is an artifact of the classical approximation that does not apply to real systems. However, the discussion above is based on the energy relaxation of the intramolecular vibrational modes that are related to the chain deformation of n-hexane. Considering that the vibrational frequencies of these modes are relatively low, we believe that the classical approximation for these modes holds at least qualitatively well.

Another point to be discussed is the difference in $G_s'(\omega)$ of the two liquids. One of us (Yamaguchi) and co-workers, measured the complex shear viscosity of various lubrication oils in the MHz regime by means of a QCM-D-based method.[46] It was found that the shear moduli of liquids with ring structures are larger than those of liquids with chain structures. The difference between $G_s'(\omega)$ of n-hexane and of cyclohexane is thus in harmony with their experimental results. We consider there are two possible reasons for the difference in the shear modulus. The first one is that the packing fraction of cyclohexane is higher than that of n-hexane at the same ambient pressure, as can be inferred from the difference in their densities shown in Table I. The second one is the difference in the rigidity of the molecule itself. Provided that the shear modulus means the rigidity of the liquid against shear deformation, it seems intuitively natural that the liquids composed of molecules of a more rigid structure exhibit larger shear modulus.

IV. SUMMARY

The sound dispersion of four liquids, *n*-hexane, cyclohexane, EGDME, approve and 1,4-dioxane, was measured in the nm^{-1} wavenumber regime by means of IXS spectroscopy. Fast sound was observed in all the liquids, that is, the sound velocity in the nm^{-1} regime was faster than that of the hydrodynamic limit. The degree of the positive dispersion of the longitudinal modulus was larger in liquids with ring structures (cyclohexane and 1,4-dioxane) than those with chain structures (*n*-hexane and EGDME), and the effect of the introduction of ether groups was rather marginal.

MD simulation of *n*-hexane and cyclohexane was also performed to clarify the difference between liquids of ring and chain structures. The sound velocity in the nm^{-1} regime was reproduced by simulation, and the difference in the degree of the fast sound was ascribed to the excess longitudinal modulus in the $q = 0$ limit. The excess longitudinal modulus was then divided into the contributions of the shear modulus and the excess volume modulus, and the latter was further divided into the rigid and vibrational energy relaxation parts. The differences in contributions of both the vibrational energy relaxation and the shear modulus were mainly responsible for the larger excess longitudinal modulus of cyclohexane. The larger shear modulus of cyclohexane was in harmony with previous works on shear relaxation of various lubrication oils and interpreted due to the higher rigidity of the molecular structure and the higher packing fraction. The smaller contribution of the vibrational energy relaxation to the excess volume modulus of *n*-hexane was ascribed to the fast energy relaxation of intramolecular vibrational modes associated with chain deformation.

The combination of IXS spectroscopy and MD simulation carried out in this work succeeded in relating the differences in dynamic properties of liquids, including frequency-dependent shear and volume viscosities, to those in molecular structures, which we believe demonstrates high potential capability of IXS spectroscopy to analyze dynamic properties of liquids, and its systematic application to various liquid systems would be fruitful in future studies.

SUPPLEMENTARY MATERIAL

See the supplementary material for the examples of the fitting of the intermediate scattering functions from MD simulation using the model function, Eq. (5).

ACKNOWLEDGMENTS

AUTHOR DECLARATIONS

Conflict of Interest

The authors have no conflicts to disclose.

Author Contributions

Tsuyoshi Yamaguchi: Conceptualization (equal); Data curation (equal); Formal analysis (equal); Investigation (equal); Methodology (equal); Visualization (equal); Writing – original draft (lead); Writing – review & editing (equal). **Koji Yoshida**: Investigation (equal); Project administration (equal); Resources (equal); Writing – review & editing (equal). **Shinya Hosokawa**: Investigation (equal); Methodology (equal); Resources (equal). **Daisuke Ishikawa**: Investigation (equal); Methodology (equal). **Alfred Q. R. Baron**: Investigation (equal); Methodology (equal); Resources (equal); Software (equal); Validation (equal); Writing – review & editing (equal).

DATA AVAILABILITY

The data that support the findings of this study are available from the corresponding author upon reasonable request.

REFERENCES

[1] J.-P. Hansen and I. R. McDonald, *Theory of Simple Liquids*, 2nd ed. (Academic Press, London, 1986).

[2] R. B. Bird, W. E. Stewart, and E. N. Lightfoot, *Transport Phenomena*, 2nd ed. (Wiley, New York, 2007).

[3] T. Yamaguchi, T. Yonezawa, and S. Koda, Phys. Chem. Chem. Phys. **17**, 19126 (2015).

[4] T. Yamaguchi, T. Yonezawa, K. Yoshida, T. Yamaguchi, M. Nagao, A. Faraone, and S. Seki, J. Phys. Chem. B **119**, 15675 (2015).

[5] T. Yamaguchi, J. Chem. Phys. **145**, 194505 (2016).

[6] T. Yamaguchi, M. Saito, K. Yoshida, T. Yamaguchi, Y. Yoda, and M. Seto, J. Phys. Chem. Lett. **9**, 298 (2018).

[7] A. Saluja and D. S. Kalonia, AAPS PharmSciTech **5**, 68 (2004).

[8] C. E. Reed, K. K. Kanazawa, and J. H. Kaufman, J. Appl. Phys. **68**, 1993 (1990).

[9] R. Behrends and U. Kaatze, Meas. Sci. Technol. **12**, 519 (2001).

[10] U. Kaatze and R. Behrends, Int. J. Thermophys. **35**, 2088 (2014).

[11] T. Yamaguchi, S. Miyake, and S. Koda, J. Phys. Chem. B **114**, 8126 (2010).

[12] T. Yamaguchi and T. Matsuoka, Jpn. J. Appl. Phys. **61**, SG1021 (2022).

[13] D. Chakraborty, B. Uthe, E. W. Malachosky, M. Pelton, and J. E. Sader, J. Phys. Chem. Lett. **12**, 3449 (2021).

[14] B. Uthe, J. F. Collis, M. Madadi, J. E. Sader, and M. Pelton, J. Phys. Chem. Lett. **12**, 4440 (2021).

[15] U. Kaatze, T. O. Hushcha, and F. Eggers, J. Solution Chem. **29**, 299 (2000).

[16] E. Burkel, Rep. Prog. Phys. **63**, 171 (2000).

[17] T. Scopigno, G. Ruocco, and F. Sette, Rev. Mod. Phys. **77**, 881 (2005).

[18] J. Teixeira, M. C. Bellissent-Funel, S. H. Chen, and B. Dorner, Phys. Rev. Lett. **54**, 2681 (1985).

[19] F. Sette, G. Ruocco, M. Krisch, U. Bergmann, C. Masciovecchio, V. Mazzacurati, G. Signorelli, and R. Verbeni, Phys. Rev. Lett. **75**, 850 (1995).

[20] T. Kamiyama, S. Hosokawa, A. Q. R. Baron, S. Tsutsui, K. Yoshida, W.-C. Pilgrim, Y. Kiyanagi, and T. Yamaguchi, J. Phys. Soc. Jpn. **73**, 1615 (2004).

[21] K. Yoshida, N. Fukuyama, T. Yamaguchi, S. Hosokawa, H. Uchiyama, S. Tsutsui, and A. Q. R. Baron, Chem. Phys. Lett. **680**, 1 (2017).

[22] S. Hosokawa, T. Kamiyama, K. Yoshida, T. Yamaguchi, S. Tsutsui, and A. Q. R. Baron, J. Mol. Liq. **332**, 115825 (2021).

[23] T. Yamaguchi, J. Chem. Phys. **156**, 244505 (2022).

[24] M. Postigo, A. Mariano, L. Mussari, and S. Canzonieri, J. Solution Chem. **30**, 1081 (2001).

[25] S. J. Ball and J. P. M. Trusler, Int. J. Thermophys. **22**, 427 (2001).

[26] A. P. Shchemelev, V. S. Samuilov, N. V. Golubeva, and O. G. Poddubskii, J. Eng. Phys. Thermophys. **94**, 509 (2021).

[27] T. Nakagawa, J. Mol. Liq. **63**, 303 (1995).

[28] B. B. Gurung and M. N. Roy, J. Solution Chem. **35**, 1587 (2006).

[29] I. Mejri, T. Kouissi, A. Toumi, N. Ouerfelli, and M. Bounaz, J. Solution Chem. **50**, 1131 (2021).

[30] A. Q. R. Baron, SPring-8 Inf. Newsl. **15**, 14 (2010).

[31] A. Q. R. Baron, in *Synchrotron Light Sources and Free-Electron Lasers*, edited by E. Jaeschke *et al.* (Springer, Cham, 2015), p. 1.

[32] A. Q. R. Baron, in *Synch. Light Srcs. & FELS*, edited by E. Jaeschke, S. Khan, J. R. Schneider, and J. B. Hastings (Springer International Publishing, Cham, 2016), pp. 1643–1757 see also https://arxiv.org/abs/1504.01098. https://doi.org/10.1007/978-3-319-04507-8_52-2 and https://doi.org/10.1007/978-3-319-04507-8_41-2.

[33] D. Ishikawa and A. Q. R. Baron, J. Synchrotron Radiat. **28**, 804 (2021).

[34] K. Tamura, M. Inui, and S. Hosokawa, Rev. Sci. Instrum. **70**, 144 (1999).

[35] S. Hosokawa, S. Inaba, H. Uchiyama, and S. Tsutsui, Phys. Status Solidi B **257**, 2000172 (2020).

[36] M. J. Abraham, T. Murtola, R. Schulz, S. Páll, J. C. Smith, B. Hess, and E. Lindahl, SoftwareX **1–2**, 19 (2015).

[37] W. L. Jorgensen, D. S. Maxwell, and J. Tirado-Rives, J. Am. Chem. Soc. **118**, 11225 (1996).

[38] M. P. Allen and D. J. Tildesley, *Computer Simulation of Liquids* (Clarendon Press, Oxford, 1987).

[39] B. Hess, H. Bekker, H. J. C. Berendsen, and J. G. E. M. Fraaije, J. Comput. Chem. **18**, 1463 (1997).

[40] U. Essmann, L. Perera, M. L. Berkowitz, T. Darden, H. Lee, and L. G. Pedersen, J. Chem. Phys. **103**, 8577 (1995).

[41] D. Ishikawa and A. Q. R. Baron, J. Phys. Soc. Jpn. **90**, 083602 (2021).

[42] J. A. McLennan, Prog. Theor. Phys. **30**, 408 (1963).

[43] R. Zwanzig, Annu. Rev. Phys. Chem. **16**, 67 (1965).

[44] T. Yamaguchi, Phys. Chem. Chem. Phys. **24**, 12311 (2022).

[45] K. Takagi, in *Ions and Molecules in Solutions*, edited by N. Tanaka, H. Ohtaki, and R. Tamamushi (Elsevier, Amsterdam, 1983), p. 183.

[46] T. Yamaguchi, T. Akatsuka, and S. Koda, J. Phys. Chem. B **117**, 3232 (2013).